Energy 230 (2021) 120836

Contents lists available at ScienceDirect

Energy

journal homepage: www.elsevier.com/locate/energy

Investigation on sector coupling potentials of a 5th generation district heating and cooling network

Hermann Edtmayer*, Peter Nageler, Richard Heimrath, Thomas Mach, Christoph Hochenauer

Institute of Thermal Engineering, Graz University of Technology, Inffeldgasse 25b, 8010, Graz, Austria

ARTICLE INFO

Article history:
Received 15 December 2020
Received in revised form
29 April 2021
Accepted 30 April 2021
Available online 5 May 2021

Keywords:
Urban building energy modelling
5GDHC
Sector coupling
Power to heat

ABSTRACT

In this paper the development and application of an urban building energy simulation model is presented to analyse an existing 5th generation district heating and cooling network (5GDHC) with regard to possible sector coupling potentials. It was evaluated, how the heat energy production through large industrial heat pumps and the total thermal capacities of the 5GDHC network can provide flexibilities for power to heat applications.

In a first step a multi model dynamic simulation was set up using the simulation environment IDA ICE. A previously developed urban energy simulation model formed the basis to implement the special requirements of the investigated 5GDHC network. This was followed by the calibration of the multi model simulation utilising the monitoring data of the existing 5GDHC network. In a second step the flexibilities of network sub areas were systematically investigated using step response tests. This was done with respect to key performance indicators like heat-up time or electrical energy consumption as a function of different boundary conditions like indoor comfort or outdoor air temperature. The third step comprised of a cumulative network analysis using different heating setpoint control strategies to optimise the operation of the network regarding heat production costs.

1. Introduction

The energy demand and greenhouse gas emissions of cities worldwide are increasing rapidly hence climate protection, especially in urban regions, must be strongly promoted [1]. For meeting the Paris climate targets and to limit global warming below 2 °C (RCP2.6), the share of fossil-based energy production must be reduced significantly in combination with further strengthening of energy efficiency measures till 2050 [2,3]. A large share of Europe's CO_2 emissions and thus potential for climate protection measures lies in the sector of heating and cooling [4]. Therefore different sources of renewable energy production as well as low exergy waste heat have to become accessible on a large scale in a reasonable economic effort [5,6]. District heating and cooling shows high potential for contributing to future energy systems [7] and the harvest of solar energy and wind is an already fast growing contribution to the energy transition [8]. Yet integrating these volatile renewable energy sources to a large extend into the existing electrical power grid depicts a significant challenge to our energy systems. Existing technical solutions have to be developed further in order to provide the necessary system flexibilities.

In that regard the further evolution of district energy systems towards smart thermal grids [9] provide great opportunities for sustainable and flexible heat energy supply in the building sector [10,11]. As well as sector coupling, which is considered as a key concept to achieve these goals of the energy transition [12,13]. Newly developed 5th generation district heating & cooling networks (5GDHC), like discussed through Lund et al. [14]. are predestined for urban environments, where sufficient heat demand density but also the necessary waste heat sources are available [15,16]. They show a huge potential for integrating various renewables, reusing waste heat sources of different kind, lowering system temperatures, as well as integrating seasonal thermal storages, heat pumps and smart control [17–25].

During the research conducted, two major hurdles for 5GDHC networks became apparent to the research team. Firstly, for 5GDHC networks the investment costs are very high. Their infrastructure with heat transfer stations, heat pumps and seasonal storage is

* Corresponding author.
E-mail address: hermann.edtmayer@tugraz.at (H. Edtmayer).

https://doi.org/10.1016/j.energy.2021.120836

costly. Secondly, there is a 'the chicken and the egg' dilemma for new development areas where a 5GDHC network is planned to be installed. Companies or investors who want to participate request a fixed heat energy retail price offer. Without knowing the final structure of the development area, the network can't be planned in full extend and no fixed heat energy retail price offer can be made.

The novelty described in this paper intends to provide answers to both of these hurdles. One research question raised was if it is possible to open new revenues for 5GDHC networks. The use of industrial-sized heat pumps opens up opportunities for power to heat sector coupling [26,27]. As has previously been shown by Terreros et al. [28,29] flexibilities can be created through the smart use of heat pumps in combination with the systems thermal capacities. So that the advantages of the day-ahead trading or grid balancing market can be used to generate extra profits. Another interesting possibility was to reduce the peak load electricity demand of the network through peak shaving and demand side management strategies in the thermal grid [30]. Therefore, it is necessary to know the thermal flexibilities of the network and to make them accessible for smart control strategies of the industrial heat pumps. An attempt is now made to apply these approaches in a novel way to the 5GDHC network considered here.

In order to address the above described 'the chicken and the egg' dilemma, novel analysis tools are necessary. So, another research question was whether it is possible to develop a simulation framework to model the network under consideration accordingly. Various tools have already been developed for modelling district heating and cooling systems [31–35]. Also, dynamic simulation models for Urban Building Energy Modelling (UBEM) as well as spatial and energy planning methods are developed by now [36–40]. The novelty of the research work presented here lies in the application of these methods to the specific layout of 5GDHC networks.

1.1. The investigated 5GDHC network

The investigated 5GDHC supply network for a residential area in the city of Zurich, Switzerland is owned by the Family Home Cooperative Zurich (Familienheim Genossenschaft Zürich - FGZ). It consists of about 2200 residential objects with 5500 inhabitants and is located in the west of Zurich. The area is surrounded by large and small waste heat sources, such as data centers or an ice-skating rink. The heating and hot water demand of the FGZ area was originally covered by a 3rd generation fossil-fired district heating network. In 2011, the cooperative decided to transform the energy supply system to fully renewable until 2050. Based on a utility value analysis the FGZ had decided on a cross-area 5GDHC network. The description of the network in this paper is based on the state of development in the year 2019. For this year a full set of monitoring data was already available and could be used to support the investigations in this research project. The 5GDHC network is designed, built and monitored by the engineering company *Anex Ingenieure AG* which is also partner in this research project and provided the monitoring data. Fig. 1 shows the state of development of the network in the year 2019.

The main supply line of the 5GDHC network, the primary side, consists of a cold and a warm pipeline (two-pipe system) with non-insulated polyethylene pipes. This primary side connects the heat supplying data centers, the seasonal ground probe storages and the customer heat transfer stations. The water temperature in this network lies between 6 °C and 26 °C. Customer heat transfer stations with large industrial heat pumps connect this primary side with the secondary side of the network which consist of the original 3GDH network. Each of this heat transfer station supplies a sub part of the customer area. In the state of development in 2019 six customer heat transfer stations where installed to supply six sub areas. The heat pumps raise the temperature levels to a range of 45 °C–67 °C, depending on the building categories located in the sub areas. In 2019 a total heat pump capacity of 7.33 $MW_{thermal}$ was installed and about 1000 households were connected to the 5GDHC network. The transfer stations are equipped with heat buffer storages as well as the original gas and oil boiler heat supplies as backup and for covering extreme peak loads. The waste heat input for the network is provided by the excess heat of two data centers. Situated in two sub areas (Grünmatt and Zentrum Friesenberg) 266 ground probes of 250 m length each are currently used as seasonal heat storage facilities. Until 2050 the 5GDHC network is planned to be operated as an undirected ring network with almost 14 $MW_{thermal}$ heat pump capacity and the ground probe storage facilities are planned to be expanded to around 430 probes. It is also planned to integrate all useable waste heat sources, such as the ice rink. Since the FGZ network is one of the first 5GDHC networks and there was little experience available for project planning, it was equipped with comprehensive measurement technology for monitoring by *Anex Ingenieure AG*. These monitoring data is used for the calibration of the simulation framework and consisted of hourly mean values of fluid temperature and mass flow for the year 2018. The energy carrier is water for heating networks.

2. Developing the dynamic simulation framework

The layout of the dynamic simulation framework is based on a previously developed UBEM simulation model [39–43] and realized in the simulation environment IDA ICE [44]. It was fitted to the special requirements of this 5GDHC network and consists of different types of components. Firstly, each of the six customer areas are depicted by its own customer area simulation model representing the heat transfer station and the secondary side 3GDH network of the respective supply area. It is a combined model of plant model and building model.

In the plant model the heat exchange between the primary and the secondary side including the heat pump is modelled. It also contains models for the hot water storage, the secondary side district heating piping as well as the connection to the associated building model, see Fig. 2. The secondary side district heating pipe model is a simplified model to simulate the pressure and thermal losses in the piping. The building model consist of a single building with one thermal zone and approximates the real building stock which consist of several buildings. It models internal and external factors such as loads, gains, masses, construction properties or number of inhabitants including their hot water demand. Using scripting in IDA ICE the building model was designed scalable for automated shaping. So that in the following calibration step, which is described in the next part of the paper, the building model properties and such the energy demand could be adjusted to the real energy demand of the sub area using the measurement data from the FGZ network. This approach was chosen because measurement data was only available for the network connections in the transfer stations and not of the building heating systems itself. In addition, there was limited information about the properties of the building stock in the sub areas.

Each customer area simulation model delivers the demand for space heating and cooling, domestic hot water as well as all relevant system temperatures. Especially the supply and return temperatures and the mass flow rates at the coupling points of the primary and secondary sides. So, the entirety of the customer area simulation models represents the building stock and the secondary side 3GDH networks of the entire study area.

Another key component of the simulation model is the primary side network model. It connects each customer area simulation

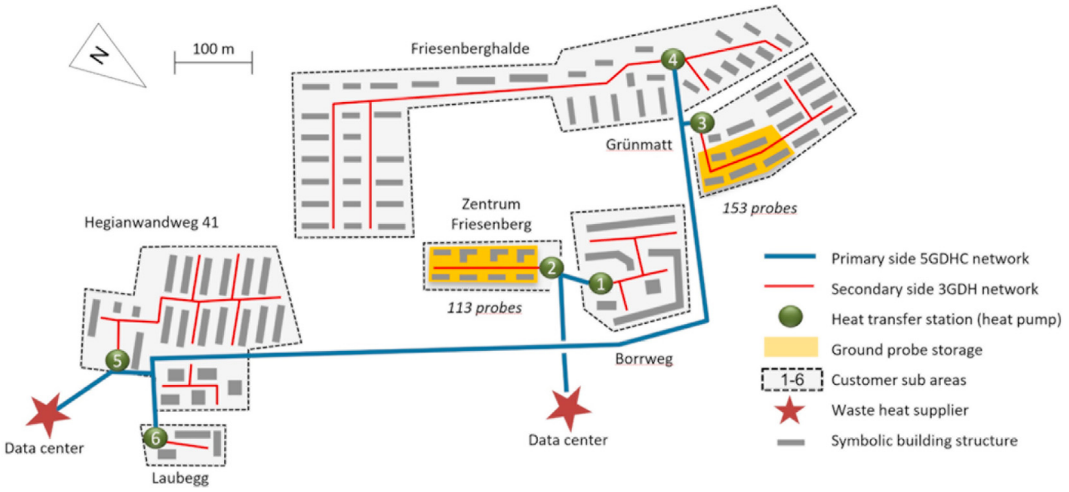

Fig. 1. Schematic layout of the 5GDHC network FGZ Zürich, state of development in 2019.

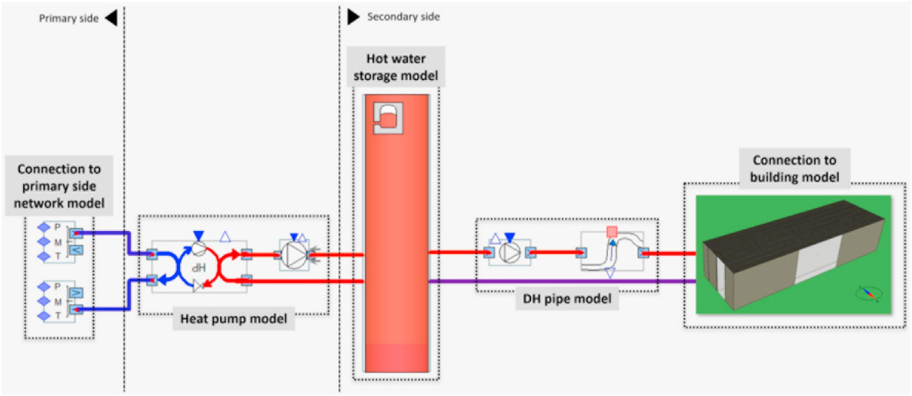

Fig. 2. Schematic layout of the plant model in the simulation framework.

model and thus each sub area of the network to the primary side network. In addition, it integrates the modelling of the waste heat sources and the ground probe storages into the network. The primary side network model enables a bidirectional mass flow in the primary heat network as well as a decentralized mass flow control by means of decentralized pumps and heat pumps at the transfer stations. In the simulation framework in each timestep the supply temperature at each transfer station is exported to the corresponding customer area simulation model and the return temperature and mass flow of each corresponding customer area simulation model is imported to the primary side network model. In addition to the simulation-relevant variables, room air temperatures of the thermal zones and the electrical power and evaporator power of the heat pumps are also imported to the primary side network model.

2.1. Calibration of the dynamic simulation framework

For the calibration of the dynamic simulation framework, the IDA ICE features Parametric Runs and Graphical Scrips were used. This features support parameter studies where the parameters can be varied either individually for sensitivity analysis or simultaneously for automatic optimization. IDA ICE features also the single-target optimization tool GenOpt [45].

For the calibration of each of the six customer area simulation models GenOpt was used to optimise the parameter Sum of Squared Errors (SSE) of the annual energy consumption as the target function in the calibration, see Equation (1). The SSE was determined at each simulation timestep n out of the measured thermal energy demand $\mathbb{Y}_i$ and the simulated thermal energy demand $\widehat{\mathbb{Y}}_i$ at the heat pump evaporator in the heat transfer station.

$$SSE = \sum_{i=1}^{n} \left(\mathbb{Y}_i - \widehat{\mathbb{Y}}_i \right)^2 \quad (1)$$

The resulting SSE over the total simulation time was then used as the target parameter to optimise in GenOpt. Through the Parametric Runs tool, GenOpt was given certain parameters to vary with allowed minimum and maximum values as well as their step size. The varying parameters were modified automatically through Graphical Scrips at each simulation run. They consisted of the building dimensions, the building wall construction type and the setpoint of the room air temperature. The heating system was also sized automatically according to the expected heating demand for the building gross floor area and envelope construction heat transition coefficients. The number of inhabitants was estimated with 50 m^2 gross floor area per person and applied to scale the hot water load profile. The windows of the building were sized using average values of window to wall ratios according to TABULA data [46]. The thermal inertia of the buildings was calibrated by adding the missing floor material mass via an additional internal mass factor in

the building model. Afterwards a manual fine tuning was done using the graphs of the annual heating power and energy consumption, see Fig. 3. This was done for each heat transfer station and customer area simulation model respectively using measurement data from the year 2019. Table 1 shows some properties of the calibrated sub area models.

Fig. 3 shows the calibration graph of the customer sub area *'Hegianwandweg'* and the comparison of measured and simulated data is depicted. In the left graph the course of power and energy is shown over the simulation of a total year. The two curves of the measured (in blue) and simulated (in red) energy displayed show a very good agreement. In the right graph the course of the power of one week in January can be seen. Although the peaks of high and low loads are not matching completely there is still a satisfactory correlation between simulated and measured data.

After the calibration of the customer area simulation models were finished the calibration of the primary side network model could be done. This calibration can be divided into a thermal and a hydraulic part. The combination of the in IDA ICE available features Parametric Runs and Graphical Scripts was again used as a calibration aid. In Parametric Runs the parameters were varied and mapped to the correct locations using Graphical Scripts. In the thermal calibration, the heat transition coefficient of district heating pipelines with the same diameter were automatically optimized. Hereby the measured and the simulated temperatures of the fluid at the heat transfer stations were compared. Further measured input parameters were the fluid temperatures and the mass flow at the heat suppliers (data centers) and at the ground probe storages. The measurement data was available in hourly mean values for the year 2018. Fig. 4 shows an example of the thermal calibration results. The temperature deviation between the measurement and the simulation at all six sub area heat transfer stations are depicted. The time period is the second week in January 2019. With a maximum deviation of about 1.5 K the simulation shows a satisfying agreement to the measurement.

The challenge of the hydraulic calibration of a 5GDHC network lies in the decentralized pressure control through pumps at the heat transfer stations. Therefore, it is necessary to validate the simulation model hydraulically and ensure that the flow direction and quantity of the mass flow in the network are correct for a given consumption. This was ensured by varying the diameter of a pipe section in the ground probe storage Friesenbergplatz. The pipe diameter was calibrated to a minimum of the Sum of Squared Errors (SSE) of the measured and simulated mass flows. Fig. 5 shows the mass flow balance at the customer sub area heat transfer stations, heat suppliers and ground probe storages over the month of January. The left graph shows the measured and the right graph the simulated mass flow balance. The inputs for the calibration were the measured mass flows at the heat suppliers and the ground probe storages. The distribution of the remaining mass flows of the ground probe storages was calibrated. The mass flow deviation between measured and simulated values is shown in Fig. 6.

3. Variant study of customer SUB areas

3.1. Methodology

Subsequently the simulation framework was used to evaluate the flexibility options of the customer sub areas with respect to response behaviour and electrical energy consumption as a function of thermal comfort in the buildings. So that the quantity of the flexibilities provided are known and in a future step can be used to optimise the heat energy retail price for customers in the network.

The approach was to consider all thermal building masses and hot water masses in the supply lines including thermal storages on the secondary side as one big thermal storage system. Depending on its state of charge, this system can then be discharged or charged for certain periods of time. This thermal loading and unloading is carried out via the heat pump in the heat transfer station. The amount of electrical energy required to operate the heat pump is thus available as flexibility for sector coupling applications. For this purpose, the parameters power, time period and thus energy quantity of the thermal storage system must be determined. To be able to make statements about the state of charge of the thermal mass, reference values need to be defined. In this case, the indoor air temperature in the buildings was used as an indicator. The standard DIN EN ISO 7730 [47] specifies indoor comfort in buildings, among others with regard to temperature in three categories. It defines lower and upper limits of the indoor air temperature beyond which it can be expected that thermal comfort is no longer met for a certain percentage of residents. Category 2 is defined as a lower limit of 20 °C and an upper limit of 24 °C at which less than 10% of people are expected to feel uncomfortable. These limits now reflect the limits of the possible state of charge in which the thermal storage unit can operate. Category 2 was subsequently used for the evaluation. This indoor air temperature was calculated using the customer sub area simulation model. Fig. 7 shows in an illustration how the basic conditions for modelling the step response test of the thermal system were defined in the cooldown experiment.

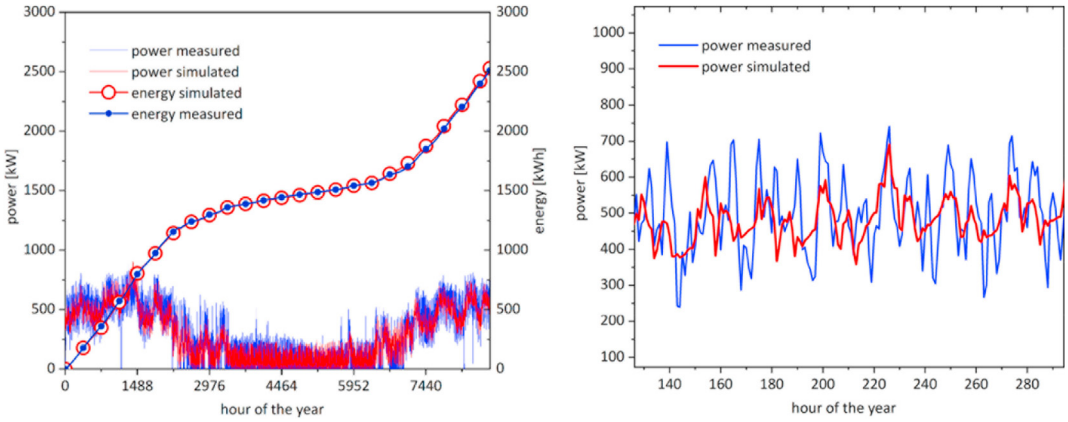

Fig. 3. Calibration graph of the customer sub area 'Hegianwandweg'; comparison of measured and simulated data; left: power and energy of the total year, right: power of one week in January.

Table 1
Properties of the calibrated sub area models.

Sub area nr. and name	Volume substitute building [m^3]	Gross floor area substitute building [m^2]	Measured total energy demand [kWh/a]	Simulated total energy demand [kWh/a]	Difference total energy demand [kWh/a]	Difference total energy demand	RMSE [kWh]
1 Borrweg	36 000	10 286	5.44E+09	5.70E+09	2.54E+08	4.6%	7.38E+04
2 Zentrum Friesenberg	81 225	23 207	4.72E+09	4.73E+09	8.63E+06	0.2%	2.60E+04
3 Grünmatt	95 510	26 431	2.61E+09	2.59E+09	1.95E+07	0.7%	4.98E+03
4 Friesenberghalde	387 500	110 714	1.82E+10	2.00E+10	1.80E+09	9.4%	2.33E+05
5 Hegianwandweg	195 533	55 870	1.18E+10	1.18E+10	2.68E+07	0.2%	1.20E+04
6 Laubegg	25 200	7200	3.32E+09	3.26E+09	6.26E+07	1.9%	1.31E+04

First, the boundary conditions for the simulation were kept constant. These included the sun-air temperature (superposition of ambient temperature and global radiation) [48], cloud cover, hot water demand, internal loads and gains, and the setpoint of the room air temperature. The simulation was kept in a constant state until the system reached a steady state. Then the heat pump was switched off and the course of the room air temperature was observed. The red curve depicts the possible course of the room air temperature in the test. Of interest was the time span until the room air temperature reached the lower limit. This corresponds to the discharge of the thermal storage from full to empty state. The simulation was stopped after reaching the lower boundary condition of the room air temperature.

With the help of the Parametric Runs tool in IDA ICE, the parameters room air temperature setpoint, sun-air temperature and cloud cover were subsequently varied. Thus, covering the spectrum of possible boundary conditions in a full factorial experiment. From this, characteristic maps could be created for variants of different building heating distribution systems. These will be presented in more detail in the next section. The same procedure was used for the heat-up test, i.e. for charging the storage system. Only difference was that at the step event in the test, the control variable of the heat pump in the model was set to the maximum. The heat pump was therefore operated at full heating capacity. These cooldown and heat-up tests were carried out with three different variants of heating distribution systems. The heat distribution via standard heating radiators served as the basic variant. As a second variant, the simulation model was equipped with floor heating and the third variant was equipped with thermal component activation.

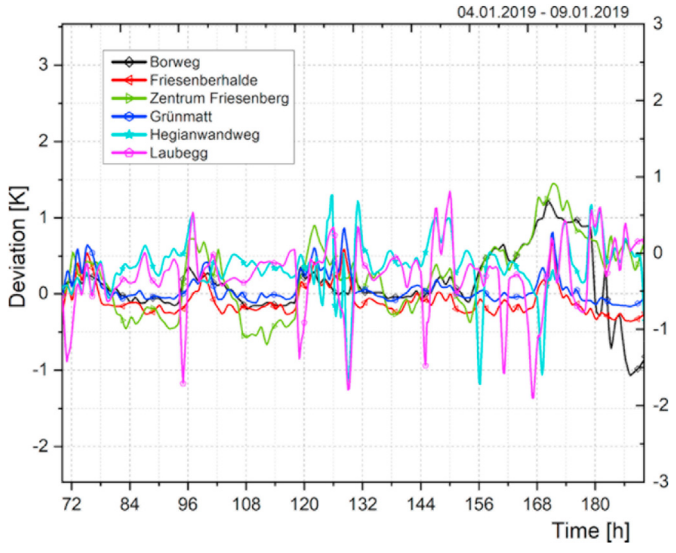

Fig. 4. Thermal calibration of the primary side network.

In order to be able to model and vary the constant boundary conditions, the outside air temperature and the global radiation were combined into a simplified sun-air temperature value. This superposition was performed according to Glück B. [48], as shown in equation (2). With $T_{sun-air}$ as the sun-air temperature calculated from the outside air temperature T_{air}, the global radiation $\dot{I}_{global}$, the absorption coefficient for short-wave solar radiation on the component surface a and the heat transfer coefficient on the component surface α_a. For the simplified consideration with constant boundary conditions, approximated values for $a = 0.5$ and $\alpha_a = 20$ were used. This results in the coefficient $\frac{a}{\alpha_a} = 0.025\ [m^2K/W]$.

$$T_{sun-air}(\tau) = T_{air}(\tau) + \frac{a\,\dot{I}_{global}(\tau)}{\alpha_a} \tag{2}$$

Fig. 8 shows the course of the calculated sun-air temperature for Zurich in the first two weeks of January 2019.

3.2. Results

The results of the step response tests are shown here using the example of the customer sub area “Hegianwandweg”. This area contains examples of all three basic classes of buildings, which are found throughout the FGZ area. Single-family buildings in the form of semi-detached houses and apartment buildings in the form of small and large multifamily building blocks. The step response tests were carried out and evaluated between 20 °C and 24 °C with regard to the comfort category 2 described above. Fig. 9 shows the course of the room air temperature in two step response tests. The water radiator supply system was used and the constant boundary conditions were set to cloudless and 0 °C sun-air temperature. The left figure shows the decay curve of the cooldown test from 24 °C to 20 °C. After switching off the heat pump, it takes about 186 min for the room air temperature to reach 20 °C.

The right figure shows the curve of the room air temperature for the heat-up test from 20 °C to 24 °C. Here the target temperature of 24 °C is reached after 78 min. In the decay curve it can be clearly seen that it takes about 1 h until the room temperature drops noticeably to 23.6 °C. In the following hour a steep drop to about 21 °C can be seen, followed by a flatter course to 20 °C in the last hour. The first shallow gradient can be explained through the hot water mass (storage tank and piping) still being well filled. In the steeper course, the heat content of the hot water mass comes to an end and in the subsequent flatter course, the heat capacity of the

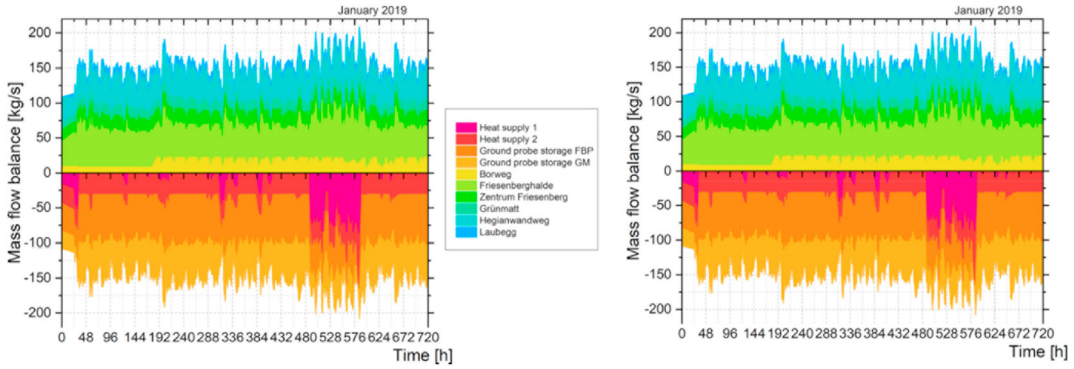

Fig. 5. Mass balance of the primary side network for January 2019. left: simulated, right: measured.

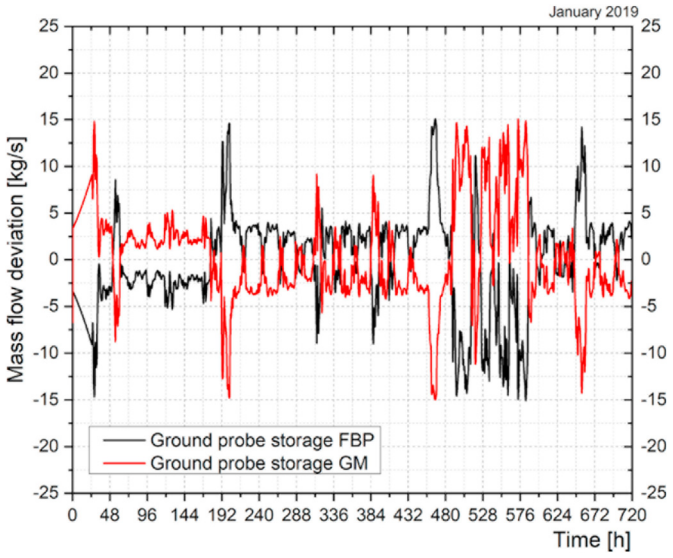

Fig. 6. Deviation of the mass flow rate between simulation and measured data in the ground probe storages for January 2019.

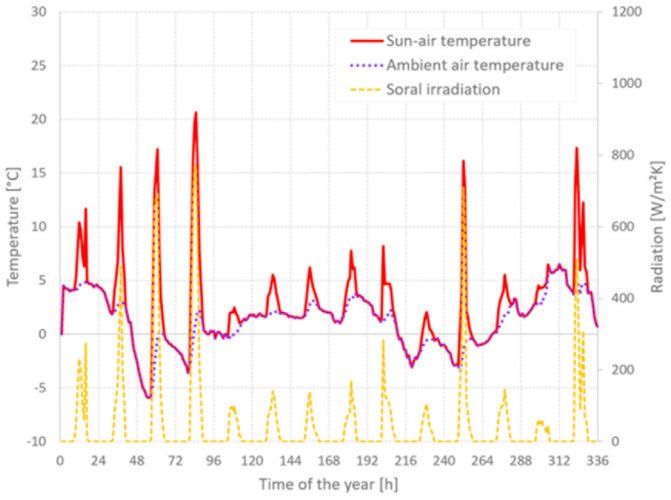

Fig. 8. Sun-air temperature for Zurich in the first two weeks of January 2019.

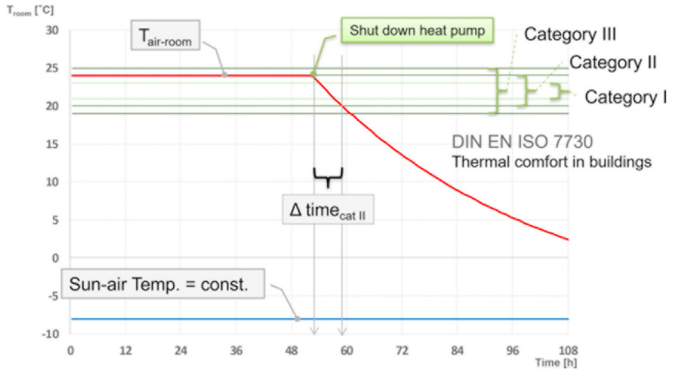

Fig. 7. Illustration of the basic conditions for modelling the step response test of the thermal system in the cooldown experiment.

building masses comes into play. This relationship is clearly illustrated in Fig. 10, which shows the water temperature curve in the hot water storage tank in the right-hand illustration. The heat-up curve in Fig. 9 shows an initial sharp rise in room air temperature in the first 30 min, followed by a flatter curve up to the target temperature of 24 °C. The course of this curve depends mainly on the heating systems radiator geometry, the supply temperature and the parameters of the heating controller. The geometry of the radiator was scaled according to the gross floor area and expected specific heat demand of the observed customer sub area. It was already set in the course of the model calibration step explained in the previous section. In addition, available system data was used to set the right supply temperature for each of the sub areas. A standard controller available in IDA ICE was used for the radiator control.

Fig. 10 again shows the step response of the building when it cools down from 24 °C to 20 °C. In this case the sun-air temperature was set to 10 °C. This results in a significantly longer cooling time of 17.8 h due to the lower heat loss of the building. The left figure shows the course of the room air temperature. The flat section from approx. hour 4 onwards shows the predominant influence of the building masses on the cooldown process over about 3/4 of the test time. This can also be clearly seen in the right-hand illustration of the temperature curve of the water temperature in the hot water storage tank. After about 3 h the temperature is only at about 25 °C and the state of charge of the hot water storage tank is almost empty. It can be clearly seen that from the beginning of the test until hour two of the shutdown, there is only a very slight drop in

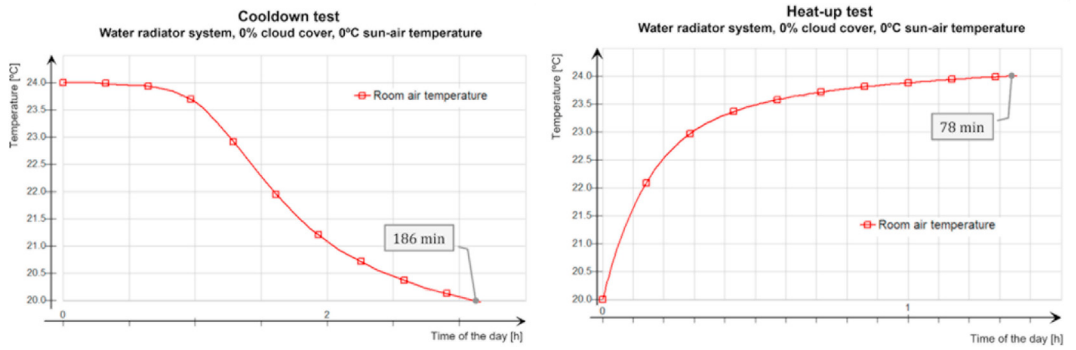

Fig. 9. Step response test with the water radiator system with 0% cloud cover and 0 °C sun-air temperature; left cooldown, right heat -up curve of the room air temperature.

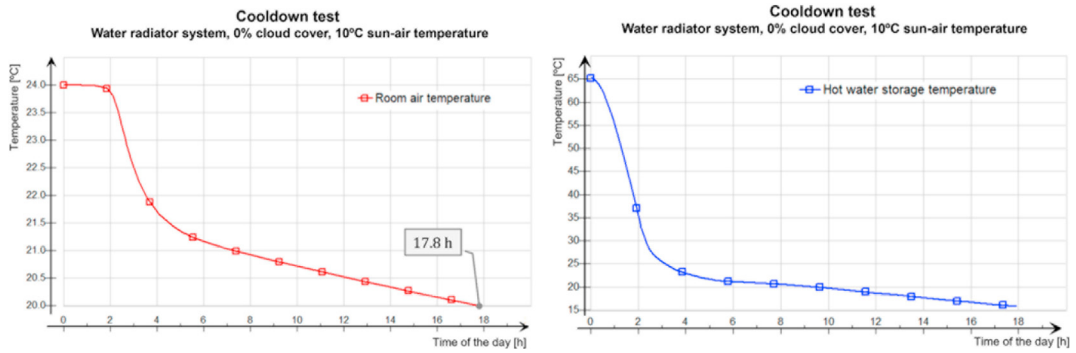

Fig. 10. Step response test with the water radiator system with 0% cloud cover and 10 °C sun-air temperature; left: room air temperature, right: hot water storage temperature.

room air temperature. This would hardly be noticed by the people in the room and would therefore not result in any loss of comfort. At 0 °C sun-air temperature, as can be seen in Fig. 9, this upper, flat area takes about 1.5 h. This area with only a slight loss of comfort could therefore be used very easily for a possible sector coupling application.

Fig. 11 shows the course of the electrical power demand of the heat pump during the heat-up test with the water radiator system. For the heat pump a standard model specified in IDA ICE was used and the parameters of the actual heat pump installed were applicated to it. It can be seen that the electrical power demand of the heat pump at the beginning of the step response test is around 300 kW. After the target room air temperature was set to 24 °C in the test the heat pump power output controller is set to the maximum value. Thus, the heat pump is operated at maximum needed thermal energy output. The electrical power consumption of the compressor initially rises sharply and approaches a value of 600 kW after approx. 10 min. This value then remains constant until the end of the step response test.

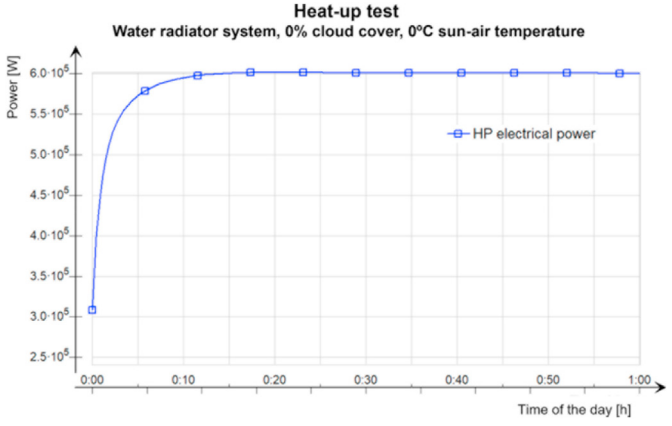

Fig. 11. Heat-up test; course of the electrical power demand of the heat pump.

Fig. 12 compares the step responses of the room air temperature when using different heat supply systems. The diagram on the left shows the heat-up tests and the diagram on the right the cooldown tests. In red with circles, both diagrams show the course of the room air temperature when using the water radiator system. In green with triangles the floor heating system and in blue with stars the heating system with thermal component activation (thermal activated floor) can be seen. A variation of the water radiator system is shown in magenta with squares. Here an extra 100 m^3 hot water volume was added to the hot water storage tank in the transfer station model. This should show the possible impact of an additional hot water storage volume on the secondary side of the network to the step response performance.

The clearly different behaviour of the various heating supply systems can be seen. In the heat-up test with the standard water radiator system, the room air temperature rises from 20 °C to 24 °C in 58 min. Compared to this, the water radiator system with additional storage is the fastest to reach the target temperature in about 50 min. An explanation is that at a constant room air temperature of 20 °C, the additional storage mass is also maintained at the supply temperature setpoint of 65 °C. If the mass flow in the heating circuit suddenly increases, a greater amount of hot water mass is available. Resulting from this the supply temperature in the heating circuit is not reduced as much as without the extra storage and a higher heating power is available. Compared to this the heating system with thermally activated floor is the slowest with 1040 min to reach the target temperature. It is clearly visible that here in the first hour

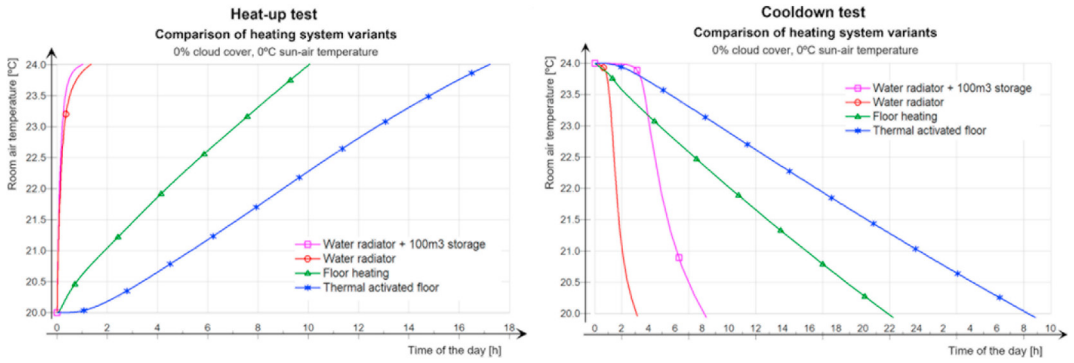

Fig. 12. Step response test, variation of heat supply systems; left: heat-up, right: cooldown.

of the test almost the entire heating energy is absorbed by the thermal mass of the floor. Afterwards the surface temperature of the floor rises slowly and a heat transfer to the air in the room can take place. In the case of the floor heating system, it can be seen that the heating power is significantly higher from the beginning on than that of the thermally activated floor and that the target temperature of 24 °C is reached after only about 600 min.

The cooldown test again shows a clear difference in behaviour between the heating system variants. Here the standard water radiator system cooled down fastest from 24 °C to 20 °C in about 180 min. The influence of the 100 m^3 of additional storage mass is even more obvious here. It takes around 240 min for the temperature in the hot water storage tank to fall, causing the room air temperature to drop noticeably. The course of the room air temperature is also flatter and thus the water radiator system with additional hot water storage tank reaches 20 °C after about 500 min. As expected, the supply system with thermally activated floor is also the one with the slowest cooldown of the room air temperature and reaches the lower limit after about 1950 min.

Figs. 13 and 14 show characteristic diagrams of values of time spans and electrical energies of the step response tests. In order to obtain these diagrams, the initial values of the room air temperature and the values of the sun-air temperature were varied full factorial in the experiment. Which means that all possible combinations of the two boundary conditions were simulated and evaluated. The initial values of the room air temperature were changed in 1 K steps and those of the sun-air temperature in 2 K steps. Again, the Parametric Runs tool in IDA ICE was used for these simulations.

The results are matrices with values at each support point of the experiment. This allows the key performance indicators (KPIs) of the sub areas, such as heat-up and cooldown time or electrical energy consumption of the heat pump to be mapped over the entire range of boundary conditions. The resulting matrices were then processed as contour plots. In Fig. 13 the characteristic diagrams of the water radiator system with the heat-up time on the left and the cooldown time on the right is shown. As can be seen from the adjacent scales, blue colours depict shorter times and red colours longer. Additionally, the values of the contour lines are shown. As an example, the map point of 21 °C room air start temperature and 0 °C sun-air temperature in the heat-up time diagram is shown. In this map point the system needs about 58 min to reach the target temperature of 24 °C. The characteristic diagram of the cooldown test shows the same. Only that the target temperature is set at 20 °C. In the map point shown of 22 °C room air start temperature and 0 °C sun-air temperature, the system reaches the target temperature after switching off the heat pump after about 120 min.

In Fig. 14 again characteristic diagrams of step response tests are shown. This time the diagrams show the electrical energy consumption of the heat pump when using different heating supply systems. Both diagrams show a heat-up test. The water radiator system on the left is compared with the floor heating system on the right. Again, shorter times are shown in blue and longer times in red and in addition the values of the contour lines are depicted. At map point 21 °C room air start temperature and 0 °C sun-air temperature, the water radiator system requires around 850 kWh of electrical energy to reach the target temperature of 24 °C. The floor heating system requires around 4700 kWh due to the greater, thermally activated storage mass. This is more than 5 times the

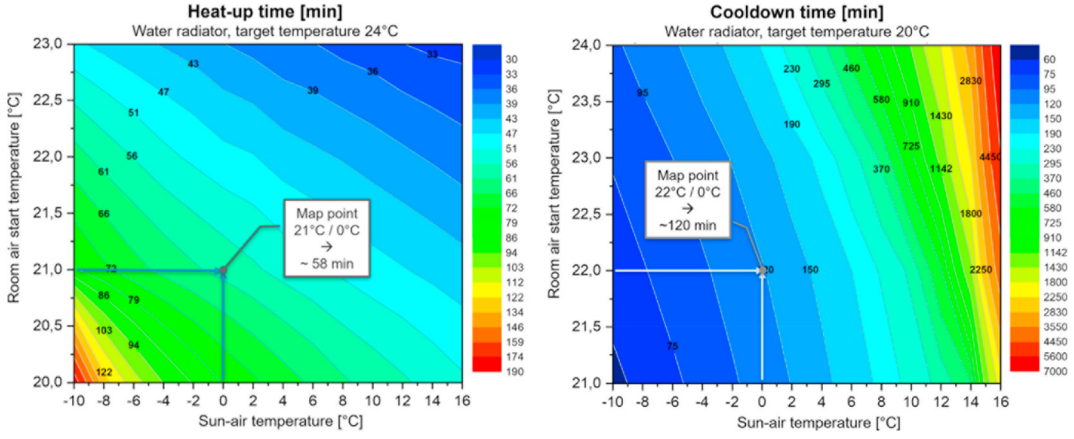

Fig. 13. Characteristic diagrams of step response times with the water radiator system; left: heat-up, right: cooldown.

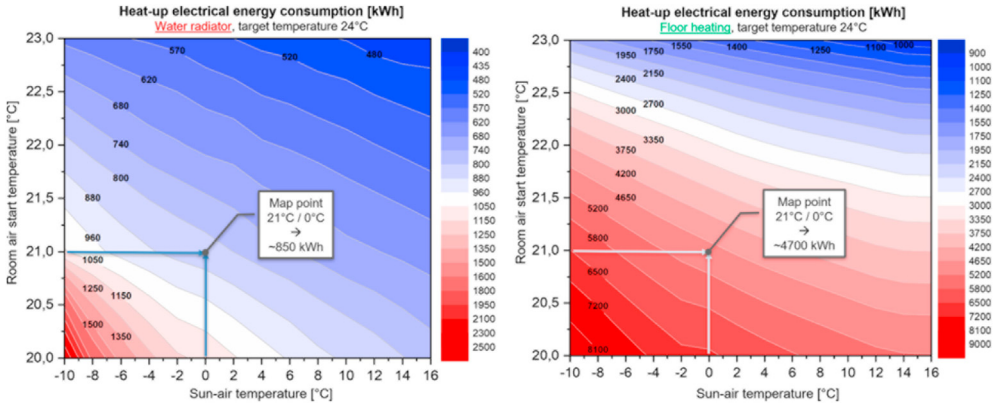

Fig. 14. Characteristic diagrams of heat-up test electrical energy consumption of the heat pump; left: water radiator system, right: floor heating system.

amount of electrical energy that can be used for a sector coupling application compared to the water radiator system.

In a next step a linear regression analysis was carried out on the matrices of the results from the step response tests. In multiple polynomial regression analysis, a dependent variable is described by several independent variables according to equation (3).

$$y = \beta_0 + \beta_1 x_1 + \beta_2 x_2 + \beta_3 x_1^2 + \ldots + \beta_i x_j^n x_l^m + \varepsilon \tag{3}$$

The software tool EES (Engineering Equation Solver) [49] was used to generate a polynomial fit of the characteristic diagrams. This results in characteristic equations, which describe the maps of the different heating supply systems by polynomials. One polynomial was derived for each KPI and heating supply system. These polynomials can now be further used for predictive models such as Model Predictive Control. It is to be mentioned that the development of predictive models was no longer part of this work. Equation (4) shows the polynomial fit of the dependent variable heat-up time τ_{heatup} with the two independent variables sun-air temperature T_{sunair} and room air start temperature T_{room} for the water radiator system. This is the fit for the left characteristic diagram in Fig. 13, using a fourth order polynomial fit including cross terms.

To assess the quality of the derived polynomials, a regression plot was created in EES. It visually indicates the goodness of the fit as well as calculates quality indicators such as the root mean square error (rmse) or the coefficient of determination. It shows the predicted value of the dependent variable obtained using the curve fit as a function of the actual value of the dependent variable for each of the datapoints that were used. Fig. 15 shows the regression plots of heat-up time of the room air temperature and electrical energy demand of the heat pump for the water radiator heating system. The red line of the plot indicates the perfect fit and therefor the scatter of the datapoints about this line is an indication about the quality of the fit. In the case of the heat-up time, the coefficient of determination is $R^2 = 98.73\%$ and the root mean square error $rmse = 8.1\ min$. In the case of the electrical energy demand, the coefficient of determination is $R^2 = 98.98\%$ and the root mean square error $rmse = 73.8\ kWh$. Both polynomials thus represent the data points from the simulation matrix with good quality.

$$\begin{aligned}\tau_{heatup} = {} & 7,6763438E^5 - 1,00022942E^4 * T_{sunair} + 3,09062582E^3 * T_{sunair}^2 - 1,57129566E^2 * T_{sunair}^3 \\ & +1,11114548E^{-3} * T_{sunair}^4 - 1,43900689E^5 * T_{room} + 1,01094396E^4 * T_{room}^2 - 3,15415066E^2 * T_{room}^3 + 3,68743801 * T_{room}^4 \\ & +1,35035532E^3 * T_{sunair} * T_{room} - 6,07598856E^1 * T_{sunair} * T_{room}^2 + 9,110866E^{-1} * T_{sunair} * T_{room}^3 \\ & -4,21894028E^2 * T_{sunair}^2 * T_{room} + 1,91868823E^1 * T_{sunair}^2 * T_{room}^2 - 2,90708331E^{-1} * T_{sunair}^2 * T_{room}^3 \\ & +2,14835891E^1 * T_{sunair}^3 * T_{room} - 9,7862508E^{-1} * T_{sunair}^3 * T_{room}^2 + 1,4850656E^{-2} * T_{sunair}^3 * T_{room}^3\end{aligned} \tag{4}$$

4. Cumulative network analysis

4.1. Methodology

In the cumulative network analysis, the calibrated overall model was used to evaluate saving potentials in the heating production costs for the 5GDHC network. The aim was to apply a peak shaving (or peak clipping) strategy on the network by using the flexibility of the thermal mass of the buildings in combination with the day-ahead electricity market price. The peaks of the parameter 'electricity cost' for the electric energy consumed by the heat pumps is tried to be reduced through the strategy. This is done by avoiding peak prices and favouring low prices for running the heat pumps. This should cut electricity costs for the operation of the heat pumps. Phases of favourable electricity prices are used to load the thermal component mass in the buildings. During phases of higher electricity prices, the loaded storage mass should be discharged, thereby reducing the electrical power demand of the heat pumps. The simulation of the entire network was carried out in a dynamic annual simulation for the year 2019. For the electricity price signal the day-ahead EPEX spot market price of Switzerland (SWISSIX) in hourly mean values for 2019 was used [50]. The hourly mean values are available in Euro/MWh. In the simulation the electricity price for a heat pump is calculated by the IDA ICE object 'Energy meter' for each timestep of the simulation using the price signal and the electricity consumption of the referring heat pump as boundary condition. The results shown in the paper are the sum of the yearly electricity costs of all heat pumps in the network.

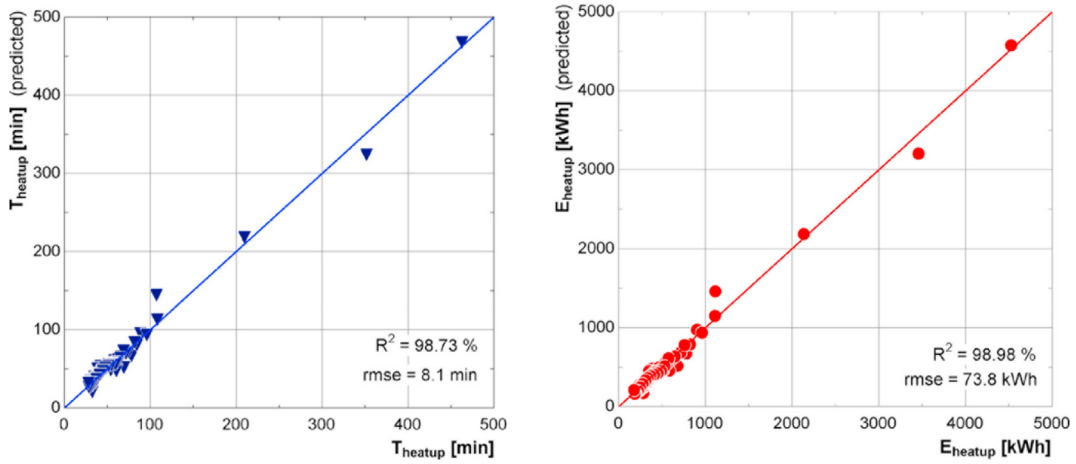

Fig. 15. Regression plot of polynomial fit functions for heat-up test characteristic diagrams; left: heat-up time, right: electrical energy consumption.

Table 2
Scenario definition for the cumulative network analysis.

Scenario	Room air temperature setpoint
Standard	22 °C
Low temperature	20 °C
High temperature	24 °C
Moving average	20–22 °C

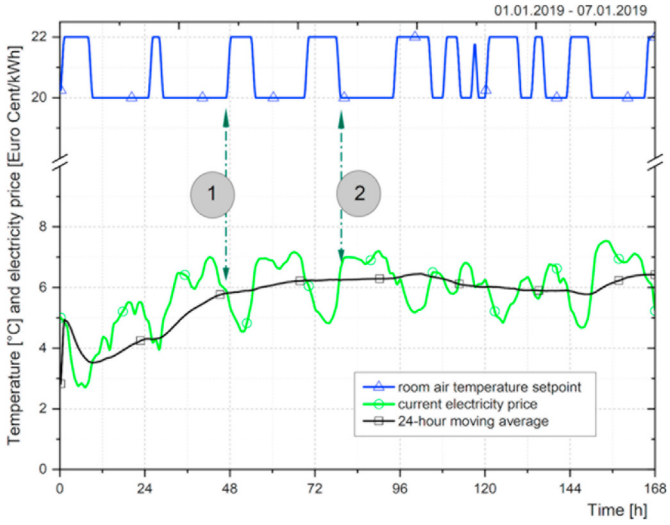

Fig. 16. Strategy for setting the room air temperature setpoint in the *Moving average scenario*.

The analysis was carried out in four different scenarios. In Table 2 the definition of the scenarios is listed.

They differ with regard to the target value of the room air temperature and the operating strategy. In the first three scenarios, the target value of the room air temperature is kept at a constant value in the simulation. In the *Standard scenario* it is set at 22 °C, in the *Low temperature scenario* at 20 °C and in the *High temperature scenario* at 24 °C. In the fourth scenario, the *Moving average scenario*, the target temperature of the room air is set variable between 20 °C and 22 °C depending on the electricity price.

Fig. 16 shows the control strategy in the *Moving average scenario* for the first week in January 2019. The setpoint of the room air temperature is depicted in blue with triangles, the course of the current electricity price in green with circles and the 24-h moving average of the electricity price in black with squares. The 24-h moving average of the electricity price was calculated by building the average of the electricity price of the past 24 h in the simulation. This was done by the IDA ICE object 'Moving average' for each timestep of the simulation using the electricity price signal as input. In this scenario, the indoor air temperature setpoint is varied between 20 and 22 °C depending on the development of the electricity price. If the current electricity price is higher than the 24-h moving average of the electricity price, the room air temperature setpoint is set to 20 °C (point #1). If the current electricity price falls below the moving average, the room air temperature setpoint is set to 22 °C (point #2). This comparison is done in each timestep of the simulation. By this procedure, periods with low electricity prices are used for charging and periods with high electricity prices for discharging the thermal storage masses of the building components.

4.2. Results

In Fig. 17 the evaporator power (left) and electrical power (right) of the heat pumps in the heat transfer stations in the *Standard scenario* are shown. In turquoise the total sum over all heat pumps is depicted and the individual heat pumps are shown in other colours.

Fig. 18 shows the comparison of the indoor thermal comfort for the scenarios. In DIN ISO 7730:2006 the indoor thermal comfort in buildings is defined between 21 °C and 23 °C at Category I. Thus, the optimum comfort value for this evaluation was defined to be at room air temperature 22 °C. The Root Mean Squared Error (RMSE) of the indoor air temperature compared to the optimum of 22 °C was formed over all customer sub areas in the annual simulation of 2019. The deviation from the optimum indoor temperature is used as an approximate measure for thermal comfort. Lower values mean higher comfort. It can be seen that the scenario with constant 24 °C performs worst. It can also be clearly seen that the moving average control strategy shows a significantly lower loss of comfort than the scenario with constant 20 °C.

Fig. 19 shows the calculated annual electricity costs for all heat pumps in the network at the left as well as corresponding profits and losses at the right. The electricity costs were calculated using the electricity price profile in hourly mean values from the Swiss

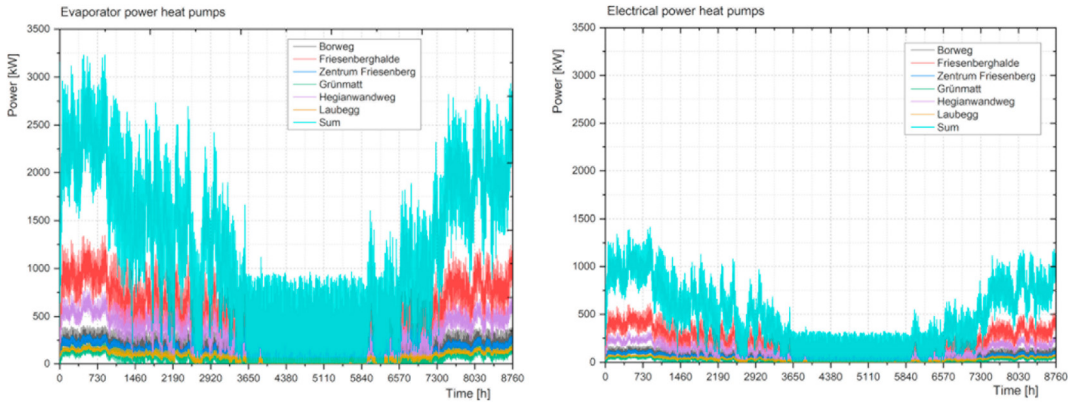

Fig. 17. Standard scenario: Evaporator power (left) and electrical power (right) of the heat pumps at the heat transfer stations.

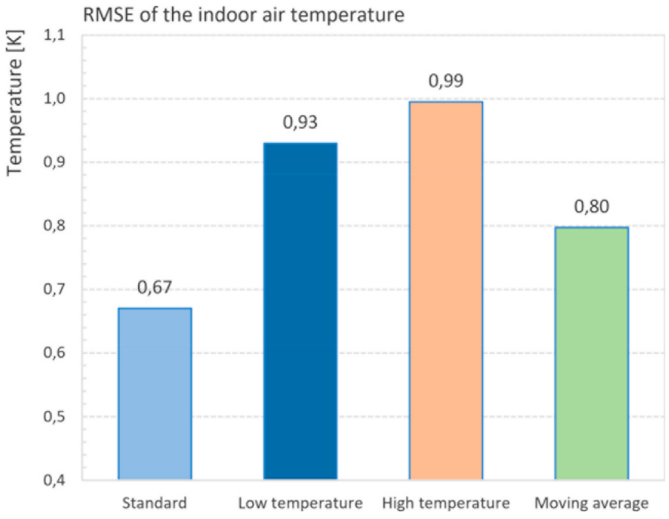

Fig. 18. Indoor comfort for the analysed scenarios; Root Mean Squared Error of the indoor air temperature to the optimum of 22 °C.

spot market *Swissix* for the year 2019. The graphs show that the electricity costs in the *Low temperature scenario*, compared to the *Standard scenario*, fall from 184 000 to 159 000€. Which corresponds to a profit of about 25 600€. But it can also be seen that the thermal comfort is significantly worse. In the *High temperature scenario*, however, the electricity costs increase to just under 211 000€. Which leads to an annual loss of about 27 300€. In comparison to the *Low temperature scenario* the comfort level drops further due to the increased number of hours above 24 °C indoor air temperature during the summer months. The scenario with the use of the moving average control strategy shows lower electricity costs of 166 000€. Which corresponds to a profit of about 18 450€ compared to the *Standard scenario*. At the same time a significantly higher level of thermal comfort can be reached compared to the *Low temperature scenario*.

Such a scenario would also be conceivable in practice by combining control with simulation in a Model Predictive Control. This coupling is necessary because on the day-ahead electricity market (or auction market), however, electricity has to be purchased 24 h in advance. This detailed forecast of the electricity demand for the next 24 h can be determined by means of an adequate thermal-electrical simulation (see e.g. Fig. 17- right).

5. Conclusion

The main research question in this investigation has been, if the investigated 5GDHC network has potential for power to heat sector coupling. And if so, how can the potential be quantified. This is linked to the second research question. Is it possible to investigate this potential using a previously developed urban building energy simulation tool on the specific topology of this network? Although there is limited amount of information about the network available.

Satisfactory answers could be found for both research questions raised. First a multi model dynamic simulation environment could be set up for the specific boundary conditions of the investigated

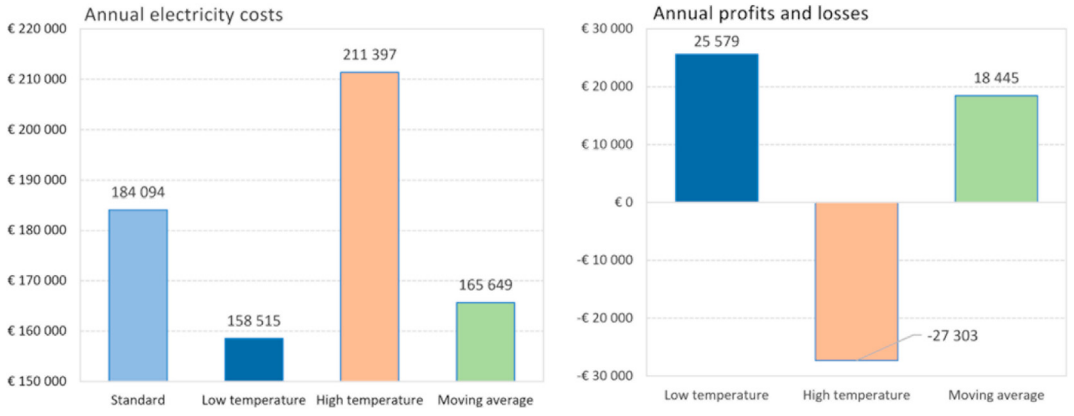

Fig. 19. Annual electricity costs (left) and the possible profits and losses (right) for the analysed scenarios.

network. This was done using the previously developed urban energy simulation tool available to the research team. All new components of this specific 5GDHC network could be implemented in the IDA ICE model and the simulation ran stably. As it is a certain issue in many comparable projects, data about the investigated network area was only partially available. There was information about the design of the primary and secondary side networks as well as the heat transfer stations. Also monitoring data of the heat transfer stations was disposable. However, no layout information or monitoring data was accessible from individual buildings connected to the network. Consequently, the modelling approach was to approximate certain consumer sub areas with single building models for which monitoring data from the existing network substations were available. These building models were then calibrated with the monitoring data, adjusting parameters such as dimensions or wall structures. A similar approach was chosen for the network model. However, the available data was more extensive and the network could be modelled in detail. Here, too, the simulation was calibrated with the real measurement data. As a result, the calibration showed a satisfactorily low amount of error between measurement and simulation. Thus, the chosen approach was seen as reliable and the consumer sub area models in combination with the network model were considered representative for this investigation.

In the following, the research question regarding the sector coupling potential of the investigated network could also be addressed. Therefore, a sensitivity analysis was carried out with the use of the developed simulation model in order to investigate the flexibilities of one specific network sub area. Various key performance indicators (KPIs) such as cooldown or heat up times of the indoor air temperature in the buildings or the electrical power and energy demand of the heat pumps could be determined from the simulation. This could be done for four different heating distribution systems as well as for varying outdoor boundary conditions of air temperature and solar radiation. The aim was to evaluate the effects of different thermally activated masses and thermal energy input and loss of the buildings on the electric energy and power demand of the heat pumps. With the used step response tests the flexibilities could be put into numbers for the targeted KPIs. And so, it could be stated that the investigated 5GDHC network shows considerable potential for power to heat sector coupling. Especially, as expected, configurations with greater thermally activated masses offer higher flexibilities. They can be used to participate in the balancing energy market or to purchase the required electrical energy on the spot market at the most favourable conditions.

Additionally, a comprehensive full factorial analysis could be performed for all sampling points of the outdoor boundary conditions. From this, matrices could be derived and characteristic diagrams of the KPIs could be generated. Furthermore, a linear regression analysis of the matrices of these results was performed. Resulting in a polynomial equation describing each KPI. The retrieved characteristic diagrams and polynomials can be used in future research work to be implemented in predictive control models for the investigated network.

In a cumulative analysis of the total network, the comparison of different control strategies was investigated. A smart control of the heating setpoint in the buildings led to a peak shaving (or peak clipping) behaviour of the control. And thus, to savings in electricity cost for the operation of the heat pumps. As research projects have certain limits in scope, other interesting analyses of the overall network had to be postponed to future research activities. This would be for example to reduce electricity network connection fees by clipping power demand peaks. Or to explore different control strategies in terms of revenues, comfort and user acceptance. However, the investigations showed that savings in the heat production costs would be possible with the currently installed system architecture.

Credit author statement

Hermann Edtmayer: Writing - Original Draft, Writing - Review & Editing, Conceptualization, Methodology, Validation, Methodology, Formal analysis, Investigation, Visualization. Peter Nageler: Methodology, Software, Validation, Methodology. Richard Heimrath: Conceptualization, Methodology, Formal analysis, Resources, Writing - Review & Editing, Visualization, Project administration. Thomas Mach: Supervision, Writing - Review & Editing, Funding acquisition. Christoph Hochenauer: Supervision, Writing - Review & Editing.

Declaration of competing interest

The authors declare that they have no known competing financial interests or personal relationships that could have appeared to influence the work reported in this paper.

Acknowledgement

This project (DeStoSimKaFe, FFG No.: 86501) is funded by the Austrian Climate and Energy Fund (www.klimafonds.gv.at/) and is being implemented as part of the Austrian Energy Research Programme 2017.

The authors want to thank all project partners for their ambitious contribution to the research project (www.aee-intec.at, www.anex.ch, www.energieinstitut.at, www.3f-solar.at, www.processenergysystems.com) and the anonymous reviewers for their work and constructive comments.

References

[1] UNDESA. Department of Economic and Social Affairs, Population Division. World urbanization prospects: highlights. 2019 (ST/ESA/SER.A/421). 2018.
[2] IPCC. Climate change 2014 synthesis report summary chapter for policymakers. Ipcc; 2014.
[3] Lund H. Renewable energy strategies for sustainable development. Energy 2007;32:912–9. https://doi.org/10.1016/j.energy.2006.10.017.
[4] Change IP on C. Summary for policymakers. In: Intergovernmental panel on climate change. Cambridge: Cambridge University Press; 2014. p. 1–30. https://doi.org/10.1017/CBO9781107415324.004. Clim. Chang. 2013 - Phys. Sci. Basis.
[5] Connolly D, Lund H, Mathiesen BV, Werner S, Möller B, Persson U, et al. Heat roadmap Europe: combining district heating with heat savings to decarbonise the EU energy system. Energy Pol 2014;65:475–89. https://doi.org/10.1016/j.enpol.2013.10.035.
[6] Alberg Østergaard P, Mathiesen BV, Möller B, Lund H. A renewable energy scenario for Aalborg Municipality based on low-temperature geothermal heat, wind power and biomass. Energy 2010;35:4892–901. https://doi.org/10.1016/j.energy.2010.08.041.
[7] Werner S. International review of district heating and cooling. Energy 2017;137:617–31. https://doi.org/10.1016/j.energy.2017.04.045.
[8] IEA. Renewables 2020. 2020. Paris.
[9] Lund H, Werner S, Wiltshire R, Svendsen S, Thorsen JE, Hvelplund F, et al. 4th Generation District Heating (4GDH). Integrating smart thermal grids into future sustainable energy systems. Energy 2014;68:1–11. https://doi.org/10.1016/j.energy.2014.02.089.
[10] Bačeković I, Østergaard PA. Local smart energy systems and cross-system integration. Energy 2018;151:812–25. https://doi.org/10.1016/

j.energy.2018.03.098.
[11] Lund H, Østergaard PA, Connolly D, Mathiesen BV. Smart energy and smart energy systems. Energy 2017;137:556–65. https://doi.org/10.1016/j.energy.2017.05.123.
[12] Fridgen G, Keller R, Körner MF, Schöpf M. A holistic view on sector coupling. Energy Pol 2020;147:111913. https://doi.org/10.1016/j.enpol.2020.111913.
[13] Arabzadeh V, Mikkola J, Jasiūnas J, Lund PD. Deep decarbonization of urban energy systems through renewable energy and sector-coupling flexibility strategies. J Environ Manag 2020;260:110090. https://doi.org/10.1016/j.jenvman.2020.110090.
[14] Lund H, Østergaard PA, Nielsen TB, Werner S, Thorsen JE, Gudmundsson O, et al. Perspectives on fourth and fifth generation district heating. Energy 2021;227:120520. https://doi.org/10.1016/j.energy.2021.120520.
[15] Pellegrini M, Bianchini A. The innovative concept of cold district heating networks: a literature review. Energies 2018;11:236. https://doi.org/10.3390/en11010236.
[16] Buffa S, Cozzini M, D'Antoni M, Baratieri M, Fedrizzi R. 5th generation district heating and cooling systems: a review of existing cases in Europe. Renew Sustain Energy Rev 2019;104:504–22. https://doi.org/10.1016/j.rser.2018.12.059.
[17] Boesten S, Ivens W, Dekker SC, Eijdems H. 5th generation district heating and cooling systems as a solution for renewable urban thermal energy supply. Adv Geosci 2019;49:129–36. https://doi.org/10.5194/adgeo-49-129-2019.
[18] Prasanna A, Dorer V, Vetterli N. Optimisation of a district energy system with a low temperature network. Energy 2017;137:632–48. https://doi.org/10.1016/j.energy.2017.03.137.
[19] Vetterli N, Sulzer M, Menti U-P. Five-year energy monitoring of a low-temperature heating and cooling network. 3rd Int Conf Smart Energy Syst 4th Gener Dist Heat 2017. https://doi.org/10.1016/j.egypro.2017.07.289. September:1–20.
[20] Sommer T, Sulzer M, Wetter M, Sotnikov A, Mennel S, Stettler C. The reservoir network: a new network topology for district heating and cooling. Energy 2020;199. https://doi.org/10.1016/j.energy.2020.117418.
[21] Sommer T, Sotnikov A, Sandmeier E, Stettler C, Mennel S, Sulzer M. Optimization of low-temperature networks by new hydraulic concepts. J. Phys. Conf. Ser. 2019;1343:12112. https://doi.org/10.1088/1742-6596/1343/1/012112. Institute of Physics Publishing.
[22] Zarin Pass R, Wetter M, Piette MA. A thermodynamic analysis of a novel bidirectional district heating and cooling network. Energy 2018;144:20–30. https://doi.org/10.1016/j.energy.2017.11.122.
[23] Bünning F, Wetter M, Fuchs M, Müller D. Bidirectional low temperature district energy systems with agent-based control: performance comparison and operation optimization. Appl Energy 2018;209:502–15. https://doi.org/10.1016/j.apenergy.2017.10.072.
[24] Formhals J, Feike F, Hemmatabady H, Welsch B, Sass I. Strategies for a transition towards a solar district heating grid with integrated seasonal geothermal energy storage. Energy 2021;228:120662. https://doi.org/10.1016/j.energy.2021.120662.
[25] Khosravi A, Laukkanen T, Vuorinen V, Syri S. Waste heat recovery from a data centre and 5G smart poles for low-temperature district heating network. Energy 2021;218:119468. https://doi.org/10.1016/j.energy.2020.119468.
[26] Østergaard PA, Andersen AN. Variable taxes promoting district heating heat pump flexibility. Energy 2021;221:119839. https://doi.org/10.1016/j.energy.2021.119839.
[27] Gaur AS, Fitiwi DZ, Curtis J. Heat pumps and our low-carbon future: a comprehensive review. Energy Res Soc Sci 2021;71:101764. https://doi.org/10.1016/j.erss.2020.101764.
[28] Terreros O, Spreitzhofer J, Basciotti D, Schmidt RR, Esterl T, Pober M, et al. Electricity market options for heat pumps in rural district heating networks in Austria. Energy 2020;196:116875. https://doi.org/10.1016/j.energy.2019.116875.
[29] Terreros O, Spreitzhofer J, Basciotti D, Esterl T, Schmidt R-R, Natiesta T, et al. Sondierung zur Realisierung des Wärmepumpenpooling für städtische Wärmenetze. Berichte Aus Energie- Und Umweltforsch 2019. 50/2019.
[30] Guelpa E, Verda V. Demand response and other demand side management techniques for district heating: a review. Energy 2021;219:119440. https://doi.org/10.1016/j.energy.2020.119440.
[31] O'Donovan K, Pertschy R, Schweiger G, Leusbrock I, Streicher W, Engel G, et al. District energy systems: modelling paradigms and general-purpose tools. Energy 2018;164:1326–40. https://doi.org/10.1016/j.energy.2018.08.193.
[32] Schweiger G, Heimrath R, Nageler P, O'Donovan K, Salzmann M, Schrammel H, et al. Tools and methods for modelling district heating systems : a comprehensive comparison. 3rd Int Conf Smart Energy Syst 4th Gener Dist Heat 2017:1–34.
[33] Schweiger G, Larsson PO, Magnusson F, Lauenburg P, Velut S. District heating and cooling systems – framework for Modelica-based simulation and dynamic optimization. Energy 2017;137:566–78. https://doi.org/10.1016/j.energy.2017.05.115.
[34] Schweiger G, Heimrath R, Falay B, O'Donovan K, Nageler P, Pertschy R, et al. District energy systems: modelling paradigms and general-purpose tools. Energy 2018;164:1326–40. https://doi.org/10.1016/j.energy.2018.08.193.
[35] Nord N, Shakerin M, Tereshchenko T, Verda V, Borchiellini R. Data informed physical models for district heating grids with distributed heat sources to understand thermal and hydraulic aspects. Energy 2021;222:119965. https://doi.org/10.1016/j.energy.2021.119965.
[36] Yazdanie M, Orehounig K. Advancing urban energy system planning and modeling approaches: gaps and solutions in perspective. Renew Sustain Energy Rev 2021;137:110607. https://doi.org/10.1016/j.rser.2020.110607.
[37] Prataviera E, Romano P, Carnieletto L, Pirotti F, Vivian J, Zarrella A. EUReCA: an open-source urban building energy modelling tool for the efficient evaluation of cities energy demand. Renew Energy 2021;173:544–60. https://doi.org/10.1016/j.renene.2021.03.144.
[38] Poggi F, Firmino A, Amado M. Planning renewable energy in rural areas: impacts on occupation and land use. Energy 2018;155:630–40. https://doi.org/10.1016/j.energy.2018.05.009.
[39] Nageler P, Schweiger G, Schranzhofer H, Mach T, Heimrath R, Hochenauer C. Novel method to simulate large-scale thermal city models. Energy 2018;157:633–46. https://doi.org/10.1016/j.energy.2018.05.190.
[40] Nageler P, Heimrath R, Mach T, Hochenauer C. Prototype of a simulation framework for georeferenced large-scale dynamic simulations of district energy systems. Appl Energy 2019;252. https://doi.org/10.1016/j.apenergy.2019.113469.
[41] Nageler P, Schweiger G, Schranzhofer H, Heimrath R, Mach T, Fochler LM, et al. Co-simulation workflow for the dynamic modelling and simulation of large-scale district energy systems. In: Proc. 16th IBPSA Conf., Rome, Italy: IBPSA International building performance simulation association, ISBN 978-1-7750520-1-2.
[42] Nageler P, Schweiger G, Pichler M, Brandl D, Mach T, Heimrath R, et al. Validation of dynamic building energy simulation tools based on a real test-box with thermally activated building systems (TABS). Energy Build 2018;168:42–55. https://doi.org/10.1016/j.enbuild.2018.03.025.
[43] Nageler P, Mach T, Heimrath R, Schranzhofer H, Hochenauer C. Generation tool for automated thermal city modelling. Appl Mech Mater 2019;887:292–9. https://doi.org/10.4028/www.scientific.net/amm.887.292.
[44] EQUA Simulation AB. IDA ICE 4.8 user manual. 2018.
[45] Wetter M. GenOpt generic optimization program user manual version 3.1.1. 2016. https://simulationresearch.lbl.gov/GO/download.html.
[46] Loga T, Stein B, Diefenbach N. TABULA building typologies in 20 European countries—making energy-related features of residential building stocks comparable. Energy Build 2016;132:4–12. https://doi.org/10.1016/J.ENBUILD.2016.06.094.
[47] Arbeitsausschuss NAErg AA 7. DIN EN ISO 7730:2006-05 Ergonomics of the thermal environment - analytical determination and interpretation of thermal comfort using calculation of the PMV and PPD indices and local thermal comfort criteria. 2006 (ISO 7730:2005); German version EN ISO 7730:2005.
[48] Glück B. Dynamisches Raummodell zur wärmetechnischen und wärmephysiologischen Bewertung; Teil D. Hamburg. RUD. OTTO MEYER-UMWELT-STIFTUNG; 2005.
[49] Klein SA. Operating manual. Engineering equation solver (EES). 2007. http://www.fchart.com/ees/.
[50] EPEX spot day ahead trading Switzerland. n.d, https://www.epexspot.com/en/market-data?data_mode=table&modality=Auction&sub_modality=DayAhead&market_area=CH&product=60&delivery_date=2021-02-13&trading_date=2021-02-12. [Accessed 12 February 2021].